

# Synaptic and Myelin Plasticity and Their Synergistic Effects in Neuromorphic Networks

Xiaosong Li, Jingru Sun, *Member, IEEE*, Yichuang Sun, *Senior Member, IEEE*, Jiliang Zhang, *Senior Member, IEEE*,

**Abstract**—Plasticity is key to the trainability of neural networks and has long been a focus in the field of brain-inspired research. Currently, neuromorphic networks primarily achieve plasticity through synaptic and myelin structures. However, these two are often studied separately, limiting further enhancement of neuronal node plasticity. This paper proposes a neuron model that incorporates both synapses and myelin, designs the corresponding neuronal circuit, and introduces a method for quantifying its discharge characteristics. Through theoretical analysis, simulations, and physical experiments, we validate the effectiveness of this quantification method. Furthermore, we summarize the formation mechanisms of synaptic and myelin plasticity, clarify the differences in their respective plasticity effects, and use the quantification method to compute the response speed, power consumption, and spike firing frequency of neuronal circuits. We also analyze the impact of synaptic and myelin plasticity and their synergistic effects on these three factors. Results demonstrate that the plasticity of synapses and myelin, as well as their synergistic interaction, can significantly optimize the performance of neuron nodes: the response duration is reduced to 2.9% of its initial value, the energy consumption per spike decreases to 38.4%, and the spike firing frequency increases to 1982.6% of the baseline level. This synergy contributes to improving the computational efficiency and energy management capabilities of neuromorphic networks.

**Index Terms**—Neuromorphic networks, Memristor, Neurons, Myelination, Synapse, Mathematical models

## I. INTRODUCTION

NEUROMORPHIC computing architectures, inspired by the working principles of the brain, have become a key research direction for addressing the physical limits of hardware integration density and overcoming the bottlenecks of the Von Neumann architecture [1]–[4]. Development of neuromorphic networks relies not only on a deeper understanding of the working mechanisms of the human brain, but also benefits from the continued advancement of large-scale spiking neural networks (SNNs) of various types and hierarchical levels, along with their supporting computing platforms [5]–[9]. Plasticity is the core characteristic of neural networks,

determining learning, memory, adaptability, and energy efficiency. Whether in the biological brain, artificial neural networks, or neuromorphic computing, effectively utilizing plasticity can enhance the system’s intelligence, making it more adaptive, robust, and computationally efficient [10]–[14]. Therefore, improving plasticity is crucial for the development of large-scale neuromorphic networks.

Similar to the brain, plasticity in neuromorphic networks can be achieved through synaptic and myelin circuits. For example, by using the nonlinear properties of memristors to simulate synaptic functions, neuromorphic chips significantly outperform the latest image processing units in terms of energy efficiency and computation speed when handling images [15]–[21]. Designing myelin structures can make it easier for neuron circuit nodes to adjust spike emission frequencies and achieve plasticity beyond synapses [22]–[26]. However, in the field of neuromorphic networks, research on synaptic and myelin plasticity is mostly conducted independently.

The effects of synapses and myelin on neuronal firing characteristics are highly similar, but their underlying mechanisms differ. Synaptic plasticity primarily regulates the connection strength between pre- and postsynaptic neurons, thereby influencing membrane current and determining neuronal response speed, power consumption, and spike firing frequency [27]–[30]. In contrast, myelin plasticity affects these characteristics by altering the membrane capacitance and permeability of neurons [31], [32]. Moreover, the segmented structure formed by myelination not only reduces interference from adjacent neurons but also significantly enhances the conduction speed of spike signals [33], [34]. More importantly, synaptic and myelin plasticity do not function independently but rather interact and collaboratively regulate neuronal firing properties [35]–[37]. Therefore, in the design of neuromorphic networks, studying synaptic or myelin plasticity in isolation may fail to fully harness the computational potential of neurons. Considering their synergistic effect comprehensively can further optimize plasticity of network, improve computational efficiency, and enhance energy efficiency.

Although the research on neuromorphic networks has explored the plasticity of synapses and myelin, there are still two challenges in studying their synergistic effect. Firstly, there is a lack of a neuron model that can simultaneously describe the plasticity of both synapses and myelin. Classical unmyelinated neuron models (such as the Hodgkin-Huxley model, HH) and myelinated neuron models (such as the Frankenhaeuser-Huxley model, FH) do not simultaneously describe the plasticity of both synapses and myelin [38], [39].

This work is supported by the National Natural Science Foundation of China (62171182), Natural Science Foundation Project of Hunan(2025JJ50345), Postgraduate Scientific Research Innovation Project of Hunan Province (CX20240452), (Corresponding author: Jingru Sun).

Xiaosong Li, Jingru Sun are with the College of Computer Science and Electronic Engineering, Hunan University, Changsha 410082, China. E-mail: liguangbi@hnu.edu.cn, jt\_sunjr@hnu.edu.cn.

Yichuang Sun is with the School of Engineering and Computer Science, University of Hertfordshire, Hatfield AL10 9AB, UK. E-mail: y.sun@herts.ac.uk.

Jiliang Zhang is with the College of Integrated Circuits, Hunan University, Changsha 410082, China. E-mail: zhangjiliang@hnu.edu.cn.

This limits the design of neuron circuit nodes that simultaneously incorporate synaptic and myelin structures for studying the synergistic effect of their plasticity. Secondly, there is a lack of computation methods for key characteristics of neuron circuit nodes, such as response speed, power consumption, and spike emission frequency. This hinders the analysis of the synergistic effect between the plasticity of myelin and synaptic structures in neuron circuit nodes.

To address the above challenges, this study establishes a neuron model, designs the corresponding neuron circuit, and conducts relevant analysis to clarify the differences and synergistic effects between myelin and synaptic plasticity. The specific contributions are as follows:

- We reviewed the physiological structure and function of biological synapses and myelin. Based on the HH model, we incorporated descriptions of synaptic and myelin plasticity and proposed an adaptive growth neuron (AGN) model.
- Based on the AGN model, we designed a neuron circuit and proposed an analysis method for the response speed, power consumption, and spike firing frequency of the neuron circuit. The validity of the neuron circuit and analysis method was verified through simulations and physical experiments.
- We analyzed how synaptic and myelin structures influence the response speed, power consumption, and spike firing frequency of neuron circuits, and explained the synergistic effect between their plasticities. This provides theoretical guidance for further enhancing the plasticity of neuromorphic networks.

The rest of this paper is organized as follows. Section II primarily introduces and analyzes the mechanisms underlying the growth and function of synaptic connections and myelination in biological neurons. Section III introduces the AGN model and neuron circuit and methods for calculating neuronal circuit response speed, power consumption, and spike firing frequency. Section IV validates the effectiveness of the above methods through theoretical calculations, simulations, and physical experiments. Section V discusses the differences in the mechanisms of synaptic and myelin plasticity, as well as their synergistic effects. Section VI is the conclusion.

## II. SYNAPTIC PLASTICITY AND MYELIN PLASTICITY

In this section, we will outline the physiological structure, function, and plasticity formation mechanisms of biological synapses and myelin.

### A. Synaptic plasticity

As shown in Fig. 1(a), a biological synapse consists of a presynaptic and a postsynaptic component, which do not directly touch but are separated by a synaptic cleft. After the presynaptic neuron fires a spike, it releases neurotransmitters into the synaptic cleft. The AMPA receptor ion channels on the postsynaptic neuron then receive and activate in response. Once the receptor ion channels open, cations, primarily sodium ions, flow into the neuron, causing the membrane potential

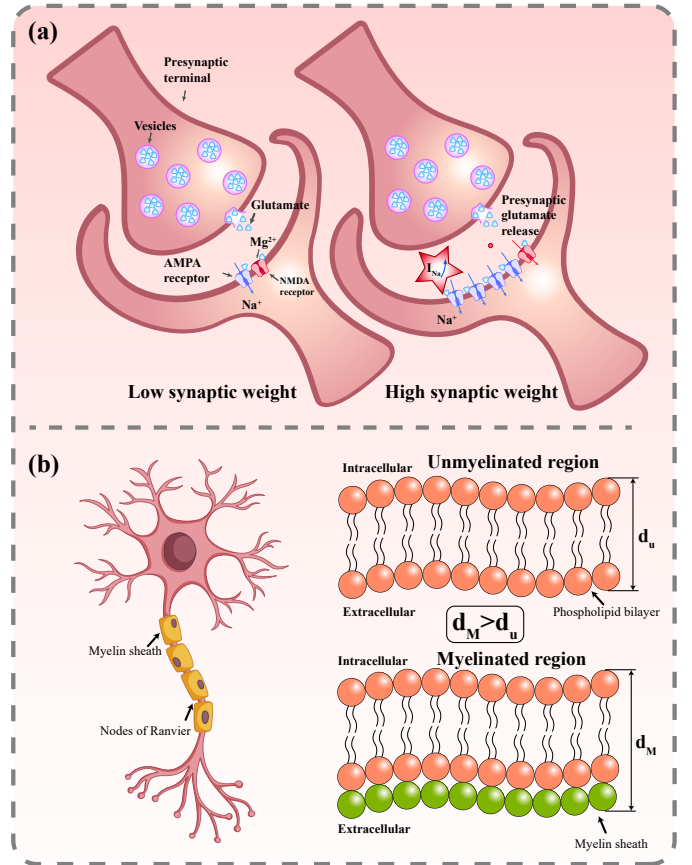


Fig. 1. The formation mechanism of biological neuronal plasticity. (a) Synaptic plasticity; (b) Myelin plasticity.

to rise and ultimately firing a spike, thereby completing the information transmission [40].

During neuronal signal transmission, the concentration of neurotransmitters in the synaptic cleft and the density of AMPA receptor ion channels on the postsynaptic neuron collectively influence information transfer efficiency. The concentration of neurotransmitters is jointly regulated by the ion concentrations inside and outside the presynaptic neuron, as well as the spike morphology (such as frequency, time intervals, etc.). This process is closely related to synaptic plasticity, but it is difficult to form memory on its own. Synaptic plasticity largely depends on the density of AMPA receptor ion channels on the postsynaptic membrane [41]. The higher the density, the greater the activation of AMPA receptor ion channels, which leads to an increased conductance, thereby amplifying the postsynaptic membrane current and making it more likely to trigger spike firing in the postsynaptic neuron [42].

In summary, to describe synaptic plasticity in the process of neuron modeling, the focus should be on the changes in synaptic weight caused by the variation in the density of AMPA receptor ion channels.

### B. Myelin plasticity

Myelin sheath is formed by Schwann cells or oligodendrocytes wrapping around the axons of neurons [43]. As shown in

Fig. 1(b), its structure is segmented. The myelinated regions provide electrical insulation, while the gaps between them are called Nodes of Ranvier. This intermittent structure enables saltatory conduction, allowing nerve signals to jump between nodes, significantly increasing transmission speed [44]. The effective thickness of the neuronal axonal membrane in the myelinated region increases, reducing membrane capacitance. Additionally, this region contains very few voltage-gated ion channels, leading to decreased ion permeability, affecting the neuron's response speed and power consumption characteristics [45]. It is worth noting that once the myelination process is complete, it is generally irreversible unless affected by pathological factors such as demyelinating diseases or other pathological mechanisms.

Incorporating myelin functionality into neuron models requires a comprehensive consideration of the enhancement in signal conduction speed due to the myelin structure, as well as the effects of the myelination process on reduced membrane capacitance and decreased membrane permeability. However, this study primarily focuses on the impact of synaptic plasticity, myelin plasticity, and their synergistic effect on neuronal response speed, power consumption, and spike firing frequency. Since synaptic plasticity does not directly affect the transmission speed of neuronal signals, the enhancement of signal transmission speed due to myelin structure is temporarily not considered in the neuron model.

### III. NEURON MODELING, CIRCUIT DESIGN, AND CHARACTERISTIC QUANTIZATION

#### A. AGN model and neuron circuit

To investigate the synergistic effects of synaptic and myelin plasticity, we propose an adaptive growth neuron (AGN) model. Eq. (1) represents the AGN's dynamics.

$$I(t) = I_c(t) + \sum_k I_k(t), \quad (1)$$

where  $I_c(t)$  and  $I_k(t)$  respectively correspond to the capacitance effect and real-time ions flow through ion channels.  $I(t)$  is the real-time total current through the axonal cell membrane. Because of myelination and membrane potential changes,  $I_c(t)$  can be further expressed as:

$$I_c(t) = \frac{C(t) \cdot dU_M(t)}{dt}, \quad (2)$$

where,  $C(t)$  represents the real-time size of the membrane capacitance, while  $\frac{dU_M}{dt}$  denotes the rate of change of the membrane potential. Since myelination causes changes in membrane capacitance, the capacitance  $C(t)$  is designed as a time-varying variable. Real-time currents flowing through each ion channel are represented by Eq. (3).

$$\sum_k I_k(t) = g_{Na}(t) \cdot (U_M(t) - U_{Na}) + g_K(t) \cdot (U_M(t) - U_K) + g_r(t) \cdot (U_M(t) - U_{Na}) + g_L(t) \cdot (U_M(t) - U_L), \quad (3)$$

where,  $g_{Na}(t)$ ,  $g_K(t)$  respectively represent the real-time conductance of each ion channel.  $U_{Na}$ ,  $U_K$ ,  $U_L$ ,  $U_r$  correspond to

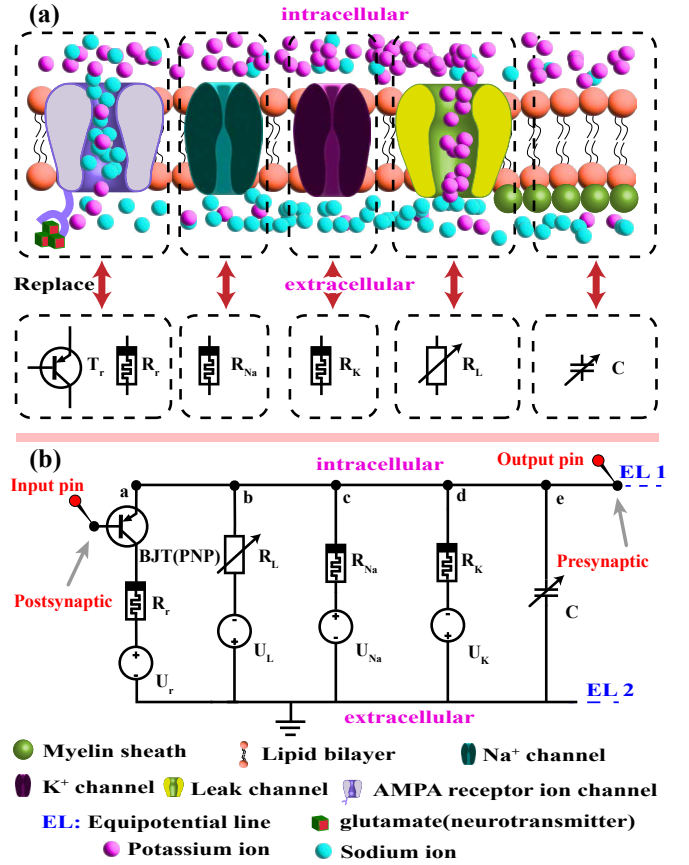


Fig. 2. (a) Neuronal key organelle physical replacement; (b) Neuronal circuit.

the Nernst potentials generated by the concentration gradients of various ions inside and outside the neuron. The  $U_M$  represents the real-time membrane potential of the neuron. In Eq. (3), we introduce  $g_r(t)$  to describe the activation characteristics of AMPA receptor ion channels, where the maximum conductance of  $g_r(t)$  is used to measure synaptic weight. Because the activation of AMPA receptor ion channels primarily involves the inward flow of cations, with  $Na^+$  being the dominant species, the Nernst potential corresponding to  $g_r(t)$  is  $U_{Na}$ . The conductance of the leak channels represents the membrane permeability of the neuron model in the resting state, denoted as  $g_L(t)$ . Since myelination affects membrane permeability,  $g_L(t)$  is also designed to vary over time.

Before designing the neuron circuit, it is necessary to determine the physical equivalent scheme for each organelle. The activation of AMPA receptor ion channels depends on their binding with neurotransmitters. Therefore, the control terminal of a three-terminal device can be used to simulate this activation characteristic. As shown in Fig. 2(a), we use a combination of MOSFET transistors and memristors to simulate AMPA receptor ion channels. The MOSFET transistor models the channel's switching behavior, representing the activation mechanism triggered by neurotransmitter binding, while the memristor simulates synaptic weight plasticity, reflecting long-term memory functions.

$Na^+$  and  $K^+$  channels are the primary channels responsible for generating action potentials in neurons, both voltage-

gated ion channels. Existing studies have employed threshold-switching memristors to simulate their voltage-dependent activation characteristics [46]–[48]. Since only the effects of myelination on membrane capacitance and membrane permeability are considered, a variable capacitor can be used to simulate changes in membrane capacitance, and a variable resistor can replace the leak channel to simulate changes in membrane permeability [25]. As shown in Fig. 2(b), the neuronal circuit is constructed based on the AGN model and the physiological structure of the neuron. The potential difference between the inside (EL1) and outside (EL2) of the neuronal circuit is the membrane potential of the neuron, denoted as  $U_M$ .

The ion channels of real biological neurons exhibit complex nonlinear dynamics, which poses challenges for circuit-level implementation. Therefore, appropriate simplification is necessary. In the ion channel design presented in this work, only the essential threshold-switching characteristics are retained—specifically, the rapid activation and inactivation of sodium channels, the rapid activation and slow inactivation of potassium channels, and the ligand-gated response of receptor ion channels to neurotransmitters—while the modeling of complex nonlinear behaviors is omitted.

### B. Synapse and myelin circuit characteristic quantization method

The plasticity of synapses and myelin can be reflected through the neuronal response speed, power consumption, and spike firing frequency. Therefore, an algorithm is needed to quantify these three attributes to effectively evaluate the plasticity of synapses, myelin, and their synergistic effect. The response speed of a neuron typically refers to the time delay between receiving the synaptic input signal and generating an action potential. The power consumption of a neuron can be evaluated based on the energy expended during the generation of a single action potential, which is typically influenced by spike firing frequency, membrane conductance, and ion channel dynamics. The spike firing frequency is the number of action potentials fired per unit time, usually expressed in Hertz ( $Hz$ ).

Time is a key parameter in calculating neuronal circuit response speed, power consumption, and spike firing frequency, with different attributes corresponding to different time metrics. The response speed is typically determined by the time from synaptic input to the neuron’s membrane potential crossing the action potential firing threshold. The quantization of power consumption and spike firing frequency involves the duration of a single action potential and the number of spikes emitted per unit of time.

However, during the generation of an action potential, multiple ion channels undergo different state transitions, leading to variations in time calculation methods. Therefore, we divide the action potential process into six stages based on the state transitions of ion channels, as shown in both Fig. 3 and Table. I. From  $t_0$  to  $t_1$  is the first stage, denoted as  $T_0$ ; from  $t_1$  to  $t_2$  is the second stage, denoted as  $T_1$ ; and so on.  $t_0$  is an arbitrary starting point in the resting state.

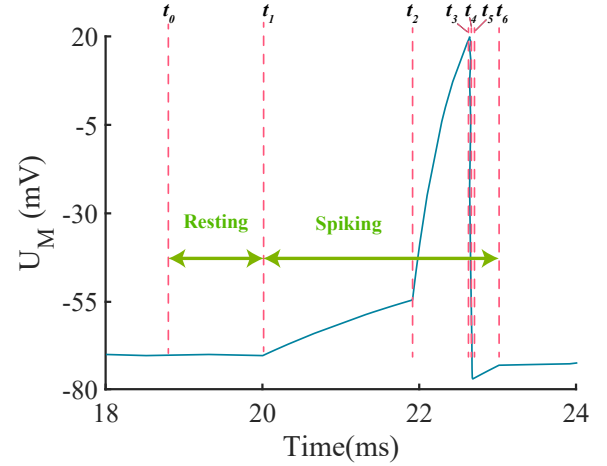


Fig. 3. The stages of an action potential.

$t_1$  represents the moment of synaptic output stimulation.  $t_2$  represents the moment when the membrane potential reaches the action potential firing threshold, at which point  $Na^+$  channels are activated.  $t_3$  represents the moment when the membrane potential reaches its maximum value, at which point the  $K^+$  channels are activated.  $t_4$  represents the moment when  $Na^+$  channels become inactivated.  $t_5$  represents the moment when the membrane potential reaches its minimum, at which point  $K^+$  channels become inactivated.  $t_6$  represents the moment when the membrane potential returns to the resting potential, at which point the action potential is completed.

To simplify the equation, we first calculate the total conductance of the neuronal circuit at each stage, denoted as  $\sigma_{zi}$  ( $i = 0, 1, 2, 3, 4, 5$ ).

$$\sigma_{zi} = \sigma_{ri} + \sigma_{Li} + \sigma_{Nai} + \sigma_{Ki}, \quad (4)$$

It is worth noting that the conductivities  $g_r, g_L, g_{Na},$  and  $g_K$  in Eq. (3), and  $\sigma_{ri}, \sigma_{Li}, \sigma_{Nai},$  and  $\sigma_{Ki}$  in Eq. (4), Eq. (6) and Eq. (8), represent the same physical quantities—the conductivities of the corresponding ion channels. The only difference lies in the notation used in different contexts:  $g$  denotes the continuous-time formulation, while  $\sigma$  represents the discretized (quantized) values at specific time steps used in numerical simulations. Their values are equivalent at corresponding moments in time. After determining the corresponding moments of  $t_0$  and  $t_1, t_i$  ( $i = 2, 3, 4, 5, 6$ ) can be calculated using Eq. (5).

$$t_i = t_{i-1} + \frac{C(t) \cdot \ln\left(1 - \frac{u_{ni} - u_{li}}{u_{hi} - u_{li}}\right)}{\sigma_{zi}}, \quad (5)$$

where,  $C(t)$  represents the membrane capacitance varying over time.  $\sigma_{ri}, \sigma_{Li}, \sigma_{Nai}$  and  $\sigma_{Ki}$  represent the conductance of their respective ion channels in the current state.  $\sigma_{Nai}$  and  $\sigma_{Ki}$  can be obtained from Table I.  $\sigma_{ri}$  and  $\sigma_{Li}$  are key variables affecting synaptic and myelin sheath plasticity, which will be listed separately in subsequent experiments.  $u_{ni}$  corresponds to the membrane potential value at  $t_{i+1}$  moment.  $u_{li}$  corresponds to the membrane potential value at  $t_i$  moment. The values of

TABLE I  
ACTIVATION STATES OF VARIOUS CHANNELS DURING CONTINUOUS SPIKE FIRING OF NEURON CIRCUIT.

No.	Stage	Time zone	Ion Channel				$u_l$	$u_n$	$U_r$	$U_L$	$U_{Na}$	$U_K$
			AMPA	Na	K	Leak						
0	$T_0$	$(t_0, t_1)$	Off( $1M\Omega$ )	Off( $1M\Omega$ )	Off( $1M\Omega$ )	On(*)	$-71mV$	$-71mV$	$55mV$	$-71mV$	$55mV$	$-77mV$
1	$T_1$	$(t_1, t_2)$	On(*)	Off( $1M\Omega$ )	Off( $1M\Omega$ )	On(*)	$-71mV$	$-55mV$	$55mV$	$-71mV$	$55mV$	$-77mV$
2	$T_2$	$(t_2, t_3)$	On(*)	On( $200\Omega$ )	Off( $1M\Omega$ )	On(*)	$-55mV$	$20mV$	$55mV$	$-71mV$	$55mV$	$-77mV$
3	$T_3$	$(t_3, t_4)$	On(*)	On( $200\Omega$ )	On( $10\Omega$ )	On(*)	$20mV$	$-64.5mV$	$55mV$	$-71mV$	$55mV$	$-77mV$
4	$T_4$	$(t_4, t_5)$	On(*)	Off( $1M\Omega$ )	On( $10\Omega$ )	On(*)	$-64.5mV$	$-74mV$	$55mV$	$-71mV$	$55mV$	$-77mV$
5	$T_5$	$(t_5, t_6)$	On(*)	Off( $1M\Omega$ )	Off( $1M\Omega$ )	On(*)	$-74mV$	$-71mV$	$55mV$	$-71mV$	$55mV$	$-77mV$

Note1 : Off( $1M\Omega$ ) represents the ion channel in an inactivated state, and the value in parentheses is the resistance corresponding to the inactivated state. Note2 : On( $200\Omega$ ) represents the ion channel in an activated state, and the value in parentheses is the resistance corresponding to the activated state. On(\*) represents the resistance in the activated state as a variable. Note3 : If only one spike is emitted, the state of AMPA receptor ion channel is “off” in the  $(t_2, t_6)$  interval.

$u_{ni}$  and  $u_{li}$  can be obtained from Table I.  $u_{hi}$  represents the final steady-state value of the membrane potential under the current ion channel state.  $u_{hi}$  can be calculated using Eq. (6).

$$u_{hi} = \frac{\sigma_{ri} \cdot U_r + \sigma_{Li} \cdot U_L + \sigma_{Nai} \cdot U_{Na} + \sigma_{Ki} \cdot U_K}{\sigma_{zi}}, \quad (6)$$

where,  $U_r, U_L, U_{Na}$  and  $U_K$  represent the Nernst potentials caused by the concentration gradients of different ions inside and outside the neuron and their values can be obtained from Table I.

The response time  $T_1$  of a neuron can be calculated using Eq. (7).

$$T_1 = t_2 - t_1. \quad (7)$$

Real-time power consumption  $P_i(t)$  ( $i = 0, 1, 2, 3, 4, 5$ ) of the neuronal circuit is influenced by the instantaneous changes in membrane potential and states of ion channel, and it can be calculated using Eq. (8).

$$P_i(t) = \sigma_{ri} \cdot (U_{Mi}(t) - U_r)^2 + \sigma_{Li} \cdot (U_{Mi}(t) - U_L)^2 + \sigma_{Nai} \cdot (U_{Mi}(t) - U_{Na})^2 + \sigma_{Ki} \cdot (U_{Mi}(t) - U_K)^2, \quad (8)$$

where,  $U_{Mi}(t)$  ( $i = 0, 1, 2, 3, 4, 5$ ) represents the real-time membrane potential of each stage. Due to the different activation states of ion channels at each stage  $T_i$  ( $i = 0, 1, 2, 3, 4, 5$ ) of the action potential, the real-time membrane potential of each phase must be calculated separately using Eq. (9).

$$U_{Mi}(t) = u_{hi} - (u_{hi} - u_{li}) \cdot \exp\left(-\frac{(t - t_i) \cdot \sigma_{zi}}{C(t)}\right). \quad (9)$$

The energy consumption  $Q_i$  ( $i = 0, 1, 2, 3, 4, 5$ ) corresponding to each stage  $T_i$  ( $i = 0, 1, 2, 3, 4, 5$ ) can be calculated using Eq. (10).

$$Q_i = \int_{t_i}^{t_{i+1}} P_i(t) dt. \quad (10)$$

In  $T_0$  stage, neuron circuit is in a resting state and does not belong to the action potential firing phase. Total energy required  $Q_z$  to fire one action potential can be calculated using Eq. (11).

$$Q_z = Q_1 + Q_2 + Q_3 + Q_4 + Q_5. \quad (11)$$

Since the parameters of the neuron circuit remain relatively constant over a short period, the spike firing frequency  $F$  can be estimated by the reciprocal of the total action potential firing time, as shown in Eq. (12).

$$F = \frac{1}{t_6 - t_1}, \quad (12)$$

#### IV. VERIFICATION OF NEURONAL CIRCUIT CHARACTERISTICS COMPUTATIONAL METHODS.

In the previous section, we proposed methods for computing the response speed, power consumption, and spike firing frequency of neuronal circuits. This section will validate the effectiveness of these methods through simulations and physical experiments.

As mentioned earlier, time is a key parameter affecting the response speed, power consumption, and spike firing frequency of neurons, especially when calculating the spike firing frequency, where the complete action potential duration needs to be considered. Therefore, to verify the accuracy of the quantization methods we proposed, we designed both simulation and physical experiments, and validated them by comparing the spike discharge frequencies from the theoretical values, simulation results, and experimental data.

##### A. Setup for PSpice simulation experiments

Neuron circuit is constructed strictly in the simulation according to the schematic diagram shown in Fig. 2(b).  $Na^+$  memristor dynamic model is given by Eq. (13), Eq. (14) and Eq. (15).  $K^+$  memristor dynamic model is given by Eq. (13), Eq. (15) and Eq. (16).

$$V(t) = (R_{off} - x \cdot \Delta R) \cdot i(t), \quad (13)$$

$$\frac{dx}{dt} = \begin{cases} -q_1 \cdot k_{on}^{b_1} \cdot f(x) \cdot i(t) \cdot \Delta R, & V(t) > V_{th1} \\ 0, & V_{th2} \leq V(t) \leq V_{th1} \\ q_2 \cdot k_{off}^{b_2} \cdot f(x) \cdot i(t) \cdot \Delta R, & V(t) < V_{th2}, \end{cases} \quad (14)$$

where,  $V(t)$  refers to the real-time voltage across the memristor.  $i(t)$  is the real-time current flowing through the memristor.  $R_{off}$  is the resistance value of the memristor in the high-resistance state,  $R_{on}$  is the resistance value in the low-resistance state, and  $\Delta R$  is the absolute difference between the

TABLE II  
 PARAMETERS OF THE MEMRISTOR MODEL.

No.	Memristor	$R_{off}$	$R_{on}$	$V_{th1}$	$V_{th2}$	$q_1$	$q_2$	$K_{on}$	$K_{off}$	$b_1$	$b_2$	$n$	$p$
1	$R_{Na}$	$1M\Omega$	$200\Omega$	$-110mV$	$-119.5mV$	1	1	4	4	10	10	—	10
2	$R_K$	$1M\Omega$	$10\Omega$	$97mV$	$7mV$	1	1	2	2	20	10	-0.002	10

two.  $x$  is the coefficient that controls the resistance variation of the memristor.  $q_1$ ,  $q_2$ ,  $b_1$ , and  $b_2$  are coefficients primarily used to control the switching speed of the memristor to match the activation and inactivation speed of ion channels.  $V_{th1}$  and  $V_{th2}$  are the switching thresholds of the memristor.  $f(x)$  is a window function that primarily constrains the coefficient  $x$  within the range  $[0, 1]$  to prevent the memristor resistance from exceeding  $R_{off}$  or dropping below  $R_{on}$ .

$$f(x) = \begin{cases} 1 - x^{2p}, & V(t) > V_{th1} \\ 1 - (x - 1)^{2p}, & V(t) \leq V_{th2}, \end{cases} \quad (15)$$

$$\frac{dx}{dt} = \begin{cases} q_1 \cdot k_{on}^{b_1} \cdot f(x) \cdot i(t) \cdot \Delta R, & V(t) > V_{th1} \\ 0, & V_{th2} \leq V(t) \leq V_{th1} \\ -q_2 \cdot k_{off}^{b_2} \cdot f(x) \cdot i(t)^n \cdot \Delta R, & V(t) < V_{th2}. \end{cases} \quad (16)$$

where,  $p$  is the key parameter controlling the nonlinear variation of the memristor, and  $n$  is a coefficient. Parameters of each memristor are listed in Table II.

Since the plasticity of myelin and synapses can be ignored when calculating the instantaneous spike firing rate of the neuron, we use fixed resistors and capacitors to replace the variable resistors and capacitors in Fig. 2(b) to simulate the effects of synapses and myelin.  $R_L$  is set to  $3k\Omega$ , and  $C$  is set to  $8\mu F$ .  $R_r$  is set to  $6k\Omega$ . The remaining parameters are provided in Table I.

### B. Setup for practical experimentation.

Consistent with the simulation experiment, the physical experiment is also designed to measure the spike firing frequency of the neuronal circuit, and the accuracy of the neuronal characteristic quantization method is verified by comparing the results with the theoretical values. The physical experimental setup is shown in Fig. 4(a). The equivalent circuit of the memristor is designed using a gated circuit to control a bidirectional thyristor switch.  $Na^+$  and  $K^+$  memristor is implemented by an equivalent circuit, as shown in Fig. 4(b). Parameters and device models involved in the PCB circuit are listed in Table III.  $R_L$  is set to  $3k\Omega$ , and  $C$  is set to  $4.4\mu F$ .  $R_r$  is set to  $10k\Omega$ . The circuit structure of the neuron circuit in the practical experiment is essentially reproduced from the simulation. The signal acquisition system is built using LabView software and an NI 6002 data acquisition card.

### C. Simulation and physical experimental results and analysis.

In the simulation, a DC voltage greater than  $20mV$  is sufficient to activate the synaptic channel and stimulate the neuron simulation circuit to continuously emit spikes. In the physical experiment, a DC voltage greater than  $2V$  can

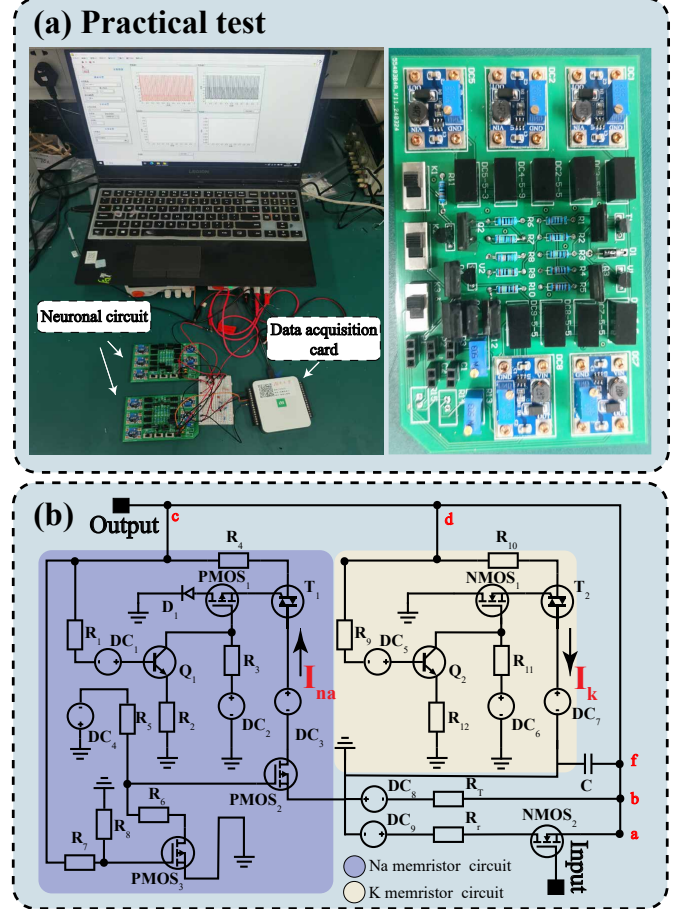


Fig. 4. (a) Practical experiment involved the PCB neuron circuitry and experimental environment; (b) PCB circuit schematic.

activate the synaptic channel and excite the neuron physical circuit to continuously emit spikes. To ensure the accuracy of spike frequency statistics, we recorded 30s of neuronal firing waveforms in both the simulation and physical experiments. The results of the simulation and physical experiments are shown in Fig. 5(a) and Fig. 5(b). To ensure clarity, only the first 400ms are displayed.

Table IV shows the simulation and physical experiments results. Data analysis indicates that the deviation between the simulation statistics and the theoretical calculations is relatively small for spike firing frequency. In contrast, the deviation between the physical experiment statistics and the theoretical calculations is comparatively larger. From Fig. 5(b), it can be observed that in the physical experiment results, the neuronal circuit's membrane potential enters a chaotic state during the short interval between two spikes, affecting the spike firing frequency. Both simulation and physical experi-

TABLE III  
PCB CIRCUIT PARAMETERS.

No.	Device	Value	Device	Value	Device	Value	Device	Value	Device	Value
1	$R_1$	$2M\Omega$	$R_2$	$100k\Omega$	$R_3$	$1M\Omega$	$R_4$	$200\Omega$	$R_5$	$10k\Omega$
2	$R_6$	$1k\Omega$	$R_7$	$1.5M\Omega$	$R_8$	$510k\Omega$	$R_9$	$2M\Omega$	$R_{10}$	$1\Omega$
3	$R_{11}$	$2M\Omega$	$R_{12}$	$200k\Omega$	$DC_1$	$6.3V$	$DC_2$	$5V$	$DC_3$	$5.5V$
4	$DC_4$	$9V$	$DC_5$	$5V$	$DC_6$	$5.5V$	$DC_7$	$7.7V$	$DC_8$	$7.1V$
5	$DC_9$	$5.5V$	$T_1$	MAC97A6	$T_2$	MAC97A6	$Q_1$	1N4007	$Q_2$	1N4007
6	$PMOS_1$	M2SJ142	$PMOS_2$	M2SJ142	$PMOS_3$	M2SJ142	$NMOS_1$	M2K946	$NMOS_2$	M2K946

TABLE IV  
SIMULATION AND PHYSICAL EXPERIMENT RESULTS.

Parameter	Simulation		Physical experiment	
	Theory	Statistics	Theory	Statistics
Spike frequency	$78.0Hz$	$76.7Hz$	$53.1Hz$	$49.6Hz$
Deviation		1.6%		6.6%

Note1 : Deviation = (Theoretical Value - Statistical Value) / Theoretical Value.

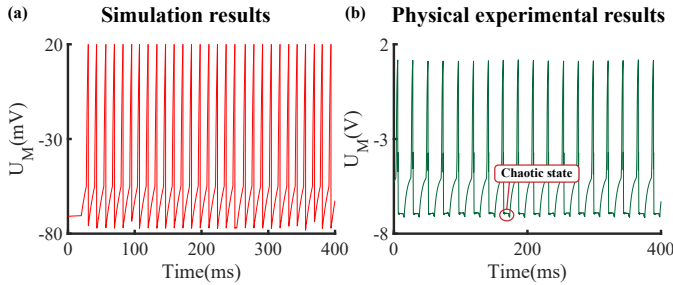


Fig. 5. (a) Simulation results; (b) Practical experiment results.

ment results indicate that the deviation between the theoretical and statistical values of the spike firing frequency is less than 10%. This validates the accuracy of the calculated duration of each stage in the neuronal circuit's action potential process and further confirms the reliability of using time-based calculations for neuronal circuit response time, power consumption, and spike firing frequency.

## V. DIFFERENCES AND SYNERGISTIC EFFECTS BETWEEN SYNAPTIC AND MYELIN PLASTICITY

This section will explore the effects of synaptic and myelin plasticity on the discharge characteristics of neuronal circuits, with a particular focus on their functional differences and synergistic effects.

### A. Differences in the Effects of Synaptic and Myelin Plasticity.

In the second subsection, we have already introduced the differences in the formation mechanisms of myelin and synaptic plasticity. Additionally, their roles in neuromorphic networks also exhibit significant differences. To better illustrate the differences in their effects, we constructed a small neuromorphic network and observed its response by adjusting synaptic and myelin plasticity to analyze their distinct influences. As shown in Fig. 6, neurons No. 1, No. 2, and No. 3, as presynaptic neurons, connect to the postsynaptic neuron No. 4 through synapses with three different weights. Parameters of

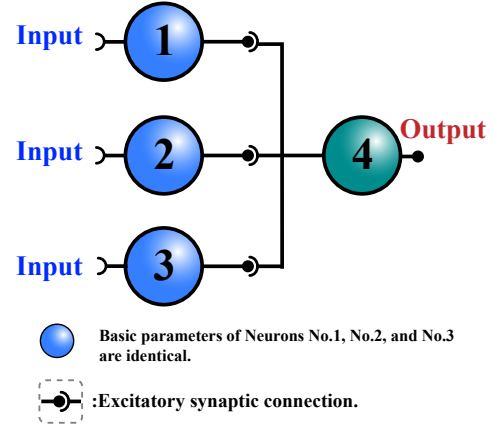


Fig. 6. Neuromorphic Network Structure Involved in Verifying the Differences Between Myelin and Synaptic Plasticity.

TABLE V  
PARAMETERS OF NEURONS IN A NEUROMORPHIC NETWORK.

No.	$R_r$	$R_L$	$C$
1	$5k\Omega$	$2.7k\Omega$	$8\mu F$
2	$5k\Omega$	$2.7k\Omega$	$8\mu F$
3	$5k\Omega$	$2.7k\Omega$	$8\mu F$
4	$R_r(1-4) : 15k\Omega$ $R_r(2-4) : 9k\Omega$ $R_r(3-4) : 4k\Omega$	Before myelination: $3k\Omega$ After myelination: $8k\Omega$	$8\mu F$ $2\mu F$

each neuron or memristor are given in Table I, Table II and Table V. Simulation was conducted in PSpice, and simulation results are shown in Fig. 7. Neurons No. 1, No. 2, and No. 3 are individually activated continuously by a  $20mV$  DC voltage (not activated simultaneously), and the simulation results are recorded for  $300ms$ , as shown in Fig. 7(a), Fig. 7(b) and Fig. 7(c). The parameter settings of Neurons No. 1, No. 2, and No. 3 are kept consistent, and they emit a spike sequence at the same fixed frequency when continuously activated.

When the synaptic weight between neurons is low, the presynaptic neuron continuously fires spikes at a low fixed frequency, but it cannot activate the postsynaptic neuron to generate spikes, as shown in Fig. 7(d) and Fig. 7(e). In this case, changes in the synaptic weight will only cause the postsynaptic membrane potential to rise, but it will not reach the threshold needed to trigger a spike. When the synaptic weight between neurons is high, even if the presynaptic neurons continue to fire spikes at the same fixed frequency, the postsynaptic neurons can be activated and generate spikes, as shown in Fig. 7(f). Additionally, the synaptic weight only

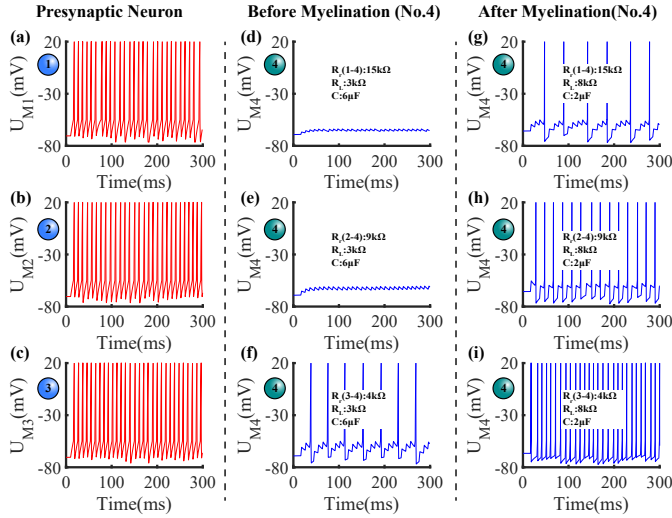


Fig. 7. Neuromorphic Network Structure Involved in Verifying the Differences Between Myelin and Synaptic Plasticity.

affects the information transfer efficiency between the pre- and post-synaptic neurons, and does not change the information transfer efficiency between the post-synaptic neuron and other neurons. In other words, synaptic plasticity establishes a one-to-one relationship in the neuromorphic network.

To better illustrate the difference between myelin plasticity and synaptic plasticity, the degree of myelination of neuron No. 4 is increased while keeping the structure of the neuromorphic network and synaptic weights unchanged, and the above simulation process is repeated. Since the parameters of neurons No. 1, No. 2, and No. 3 remain unchanged, the simulation results are consistent with previous Fig. 7(a), Fig. 7(b) and Fig. 7(c). The output results of neuron No. 4 are shown in Fig. 7(g), Fig. 7(h), and Fig. 7(j). Clearly, even though the presynaptic neurons continue to spike at a fixed frequency, the postsynaptic neurons are able to produce spikes under all three different weight connections. In other words, myelin plasticity establishes a many-to-one relationship in the neuromorphic network. The myelinated neurons become more sensitive to the stimuli from presynaptic neurons and even to noise signals. Compared to before myelination, the membrane potential fluctuations are larger under the same stimulus, and spikes are more easily generated.

In summary, synaptic plasticity establishes a one-to-one relationship in the neuromorphic network, while myelin plasticity forms a many-to-one relationship.

### B. Synergistic effect of synaptic and myelin plasticity on response speed.

Previous sections have mentioned that adjusting synaptic weight or the degree of myelination can influence the firing characteristics of the neuronal circuit. This section explores the synergistic effect between synaptic plasticity and myelin plasticity by analyzing the neuronal circuit's response speed, power consumption, and variation patterns of spike firing frequency. Since the synergistic effect between synaptic plasticity and myelin plasticity is a continuous dynamic process, we

calculate the response speed, power consumption, and spike firing frequency of the neuronal circuit under different synaptic weights and degrees of myelination based on Eq. (5), Eq. (7) and Eq. (11), to quantify their effects. To simulate the continuous firing of action potentials in neurons, the excitatory receptor ion channels are set to remain open by default during computation, with their conductance regulated by  $R_r$ . Furthermore,  $R_r$  represents the equivalent total conductance when all excitatory receptor ion channels in the neuronal circuit are activated simultaneously, thus simulating the maximum membrane current achievable through synaptic input.

The synergistic effect of synaptic plasticity and myelin plasticity on the response speed of neuronal circuits is shown in Fig. 8. When synaptic weight is low, even if receptor ion channels remain open, the response time of the neuronal circuit is still relatively long, as shown in Fig. 8(a). This is because synaptic weight is positively correlated with postsynaptic membrane current, thus prolonging the response time of the neuronal circuit. This can be verified by observing the same positions in Fig. 8(a) to Fig. 8(i). As the synaptic weight gradually increases, the maximum membrane current that synaptic input can reach continues to rise. It can be observed that the effect of myelination on reducing the response time of the neuronal circuit gradually weakens, as shown in Fig. 8(a) to Fig. 8(i). This is because the increase in membrane current caused by synaptic input has a greater effect on compressing response time than myelination, thereby diminishing the relative contribution of myelination to enhancing neuronal response speed.

As shown in Fig. 2, the neuronal circuit is essentially a relatively complex RC circuit, whose time constant  $\tau$  determines the circuit response time and can be calculated by Eq. (17).

$$\begin{aligned} \tau &= R(t) \cdot C(t) \\ &= \frac{C(t)}{\sigma_{zi}}, \\ &= \frac{C(t)}{(\sigma_{ri1} + \sigma_{ri2} + \dots + \sigma_{rin}) + \sigma_{Nai} + \sigma_{Ki} + \sigma_{Li}}, \end{aligned} \quad (17)$$

where,  $\tau$  is the time constant,  $R(t)$  is the total external-to-internal resistance of the neuronal circuit, and  $\sigma_{zi}$  ( $i = 0, 1, 2, 3, 4, 5$ ) is the total conductivity.  $C(t)$  is membrane capacitance, and  $\sigma_{Nai}$ ,  $\sigma_{Ki}$ ,  $\sigma_{Li}$  ( $i = 0, 1, 2, 3, 4, 5$ ) are the conductances corresponding to  $Na^+$ ,  $K^+$ , and leak channels, respectively.  $\sigma_{rij}$  ( $i = 0, 1, 2, 3, 4, 5$  and  $j = 0, 1, \dots, n$ ) represents the conductance of receptor ion channels corresponding to different synapses at various stages of the action potential.

In plotting Fig. 8, to clearly demonstrate the role of synaptic plasticity in the neuromorphic network, we assume that all synapses in the neuronal circuit are activated simultaneously to simulate the maximum membrane current achievable by synaptic input, thereby quantifying synaptic plasticity. However, since synaptic activation in the neuronal circuit is typically random, it is more difficult to regulate the response time of the neuronal circuit through synaptic plasticity. Eq. (17) clearly shows that the activation state of all synapses in the

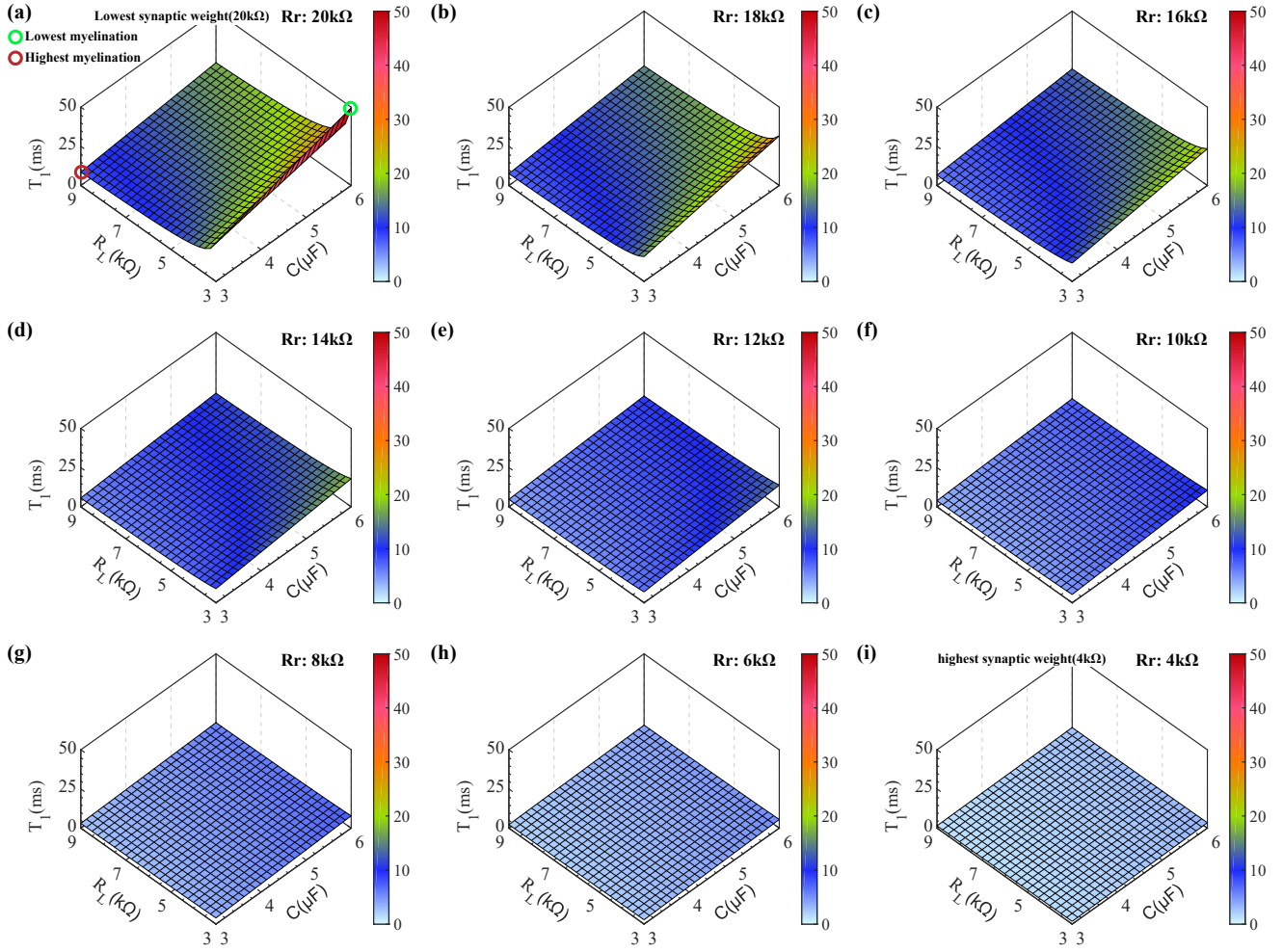


Fig. 8. The synergistic effect of synaptic plasticity and myelin plasticity on the response speed of neuronal circuits.

neuronal circuit affects the time constant, thereby influencing the response time. To adjust the response time of a specific node in the neuromorphic network through synaptic plasticity, at least one synaptic weight must be adjusted, along with the synaptic activation state. In contrast, through myelin plasticity, only the membrane permeability ( $R_L(t)$ ) and membrane capacitance ( $C(t)$ ) of the neuronal circuit need to be adjusted.

In summary, firstly, although synaptic plasticity and myelin plasticity can regulate the response time of neuronal circuits, adjusting synaptic plasticity involves more parameters and is more challenging, far exceeding the difficulty of regulating through myelin plasticity. Secondly, during the training of the neuromorphic network, by focusing on regulating myelin plasticity and supplementing with synaptic plasticity adjustments, the response speed of the neuronal circuit nodes can be adjusted more quickly and precisely. Thirdly, the combined regulation of synaptic and myelin plasticity helps further expand the control range of neuronal circuit response time, as demonstrated by comparing Fig. 8(a) and Fig. 8(i).

### C. Synergistic effect of synaptic and myelin plasticity on power consumption

Similar to biological neurons, the power consumption of the neuronal circuit differs significantly between the resting state and the action potential phase. In the resting state, receptor ion channels (synapses),  $Na^+$  channels, and  $K^+$  channels remain in an inactive state. In contrast, the activation state of the leak channel is unaffected by action potentials and remains continuously active. Since synapses are not activated in the resting state, changes in synaptic weight do not directly affect energy consumption in this state, as shown in Fig. 9(a), Fig. 9(b) and Fig. 9(c). After myelination of the neuronal circuit, the conductance of the leak channels decreases (corresponding to reduced membrane permeability), thereby influencing energy consumption in the resting state. However, if the change in leak channel conductance is small, its impact on the overall conductance of the neuron may be limited, making the effect of myelination on the energy consumption of the resting state relatively minor. Nevertheless, over a long timescale, even small changes in leak channel conductance may lead to cumulative effects on energy consumption.

We evaluate the power consumption of neuronal circuit

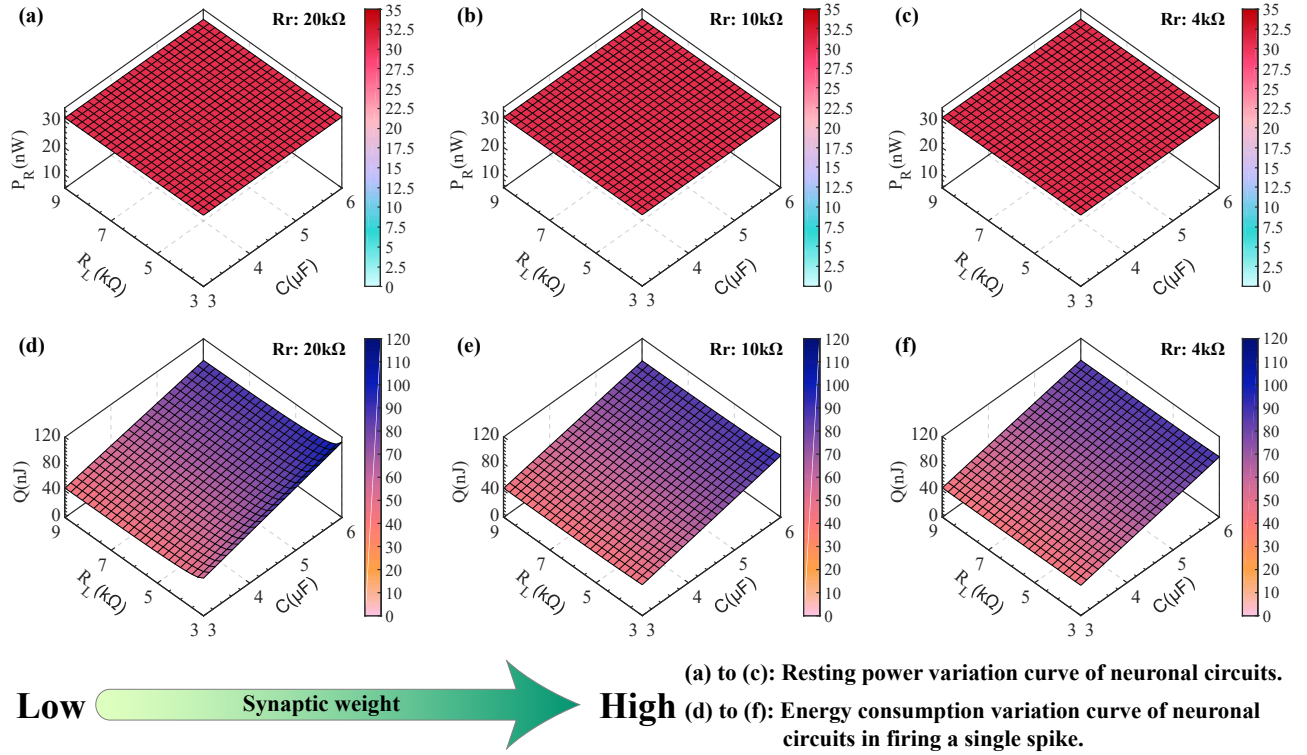


Fig. 9. The effects of synaptic plasticity and myelin plasticity on the power consumption of the neuronal circuit in resting state and action potential generation.

spike firing by calculating the energy required to generate a single action potential. As shown in Fig 9(d), Fig 9(e), and Fig 9(f), synaptic plasticity has a minimal impact on the energy consumption of a single action potential in a neuron. Calculating the power consumption of a neuronal circuit requires considering the duration of a single action potential and the membrane currents of various ion channels. An increase in synaptic weight enhances the postsynaptic membrane current, thereby accelerating the activation of ion channels and shortening the duration of the action potential. Although the increased synaptic current may lead to higher instantaneous energy consumption, the reduction in action potential duration offsets this effect. As a result, synaptic plasticity has a relatively minor impact on the total energy consumption of a single action potential.

As shown in Fig 9(d), Fig 9(e) and Fig 9(f), myelination significantly affects the energy consumption of generating a single action potential in a neuronal circuit. Compared to a high degree of myelination, a neuronal circuit with lower myelination has a larger membrane capacitance, which reduces the rate of membrane potential changes in response to the same input intensity. This prolongs the duration of the action potential, leading to increased energy consumption. Additionally, a lower degree of myelination corresponds to higher membrane permeability (i.e., higher leak channel conductance), resulting in greater membrane current leakage. This further reduces the rate of membrane potential changes, extends the action potential duration, and increases energy consumption. This phenomenon is particularly evident at low synaptic weights, as shown in Fig 9(d).

In summary, Firstly, in the resting state of the neuronal circuit, synaptic plasticity and myelin plasticity have little direct impact on circuit power consumption. Secondly, during the action potential duration, an increase in synaptic weight raises instantaneous power consumption but simultaneously shortens the duration of the action potential. As a result, synaptic plasticity has a minimal effect on the total energy consumption of a single action potential. Thirdly, as the degree of myelination in the neuronal circuit increases, the energy consumption per action potential significantly decreases. Furthermore, the synergistic effect of synaptic plasticity and myelin plasticity can reduce energy consumption while enabling the neuronal circuit to generate action potentials within a shorter time.

#### D. Synergistic effect of synaptic and myelin plasticity on spike firing frequency

As shown in Fig. 10(a) to Fig. 10(i), an increase in synaptic weight leads to a higher spike firing frequency in neurons. For the same reason that it compresses the response time of the neuronal circuit, the increase in synaptic weight results in a larger membrane current, which accelerates the rate of change in the neuron's membrane potential, thus increasing the spike firing frequency. Similarly, the spike firing frequency of the neuronal circuit is also determined by the time constant  $\tau$ . In neuromorphic networks, controlling the spike firing frequency of nodes through synaptic weights is also challenging, as it requires coordinating multiple synaptic weights and their activation sequences, involving many parameters.

Myelination plasticity can also affect the time constant of neuronal circuits. Compared to synaptic plasticity, myelination

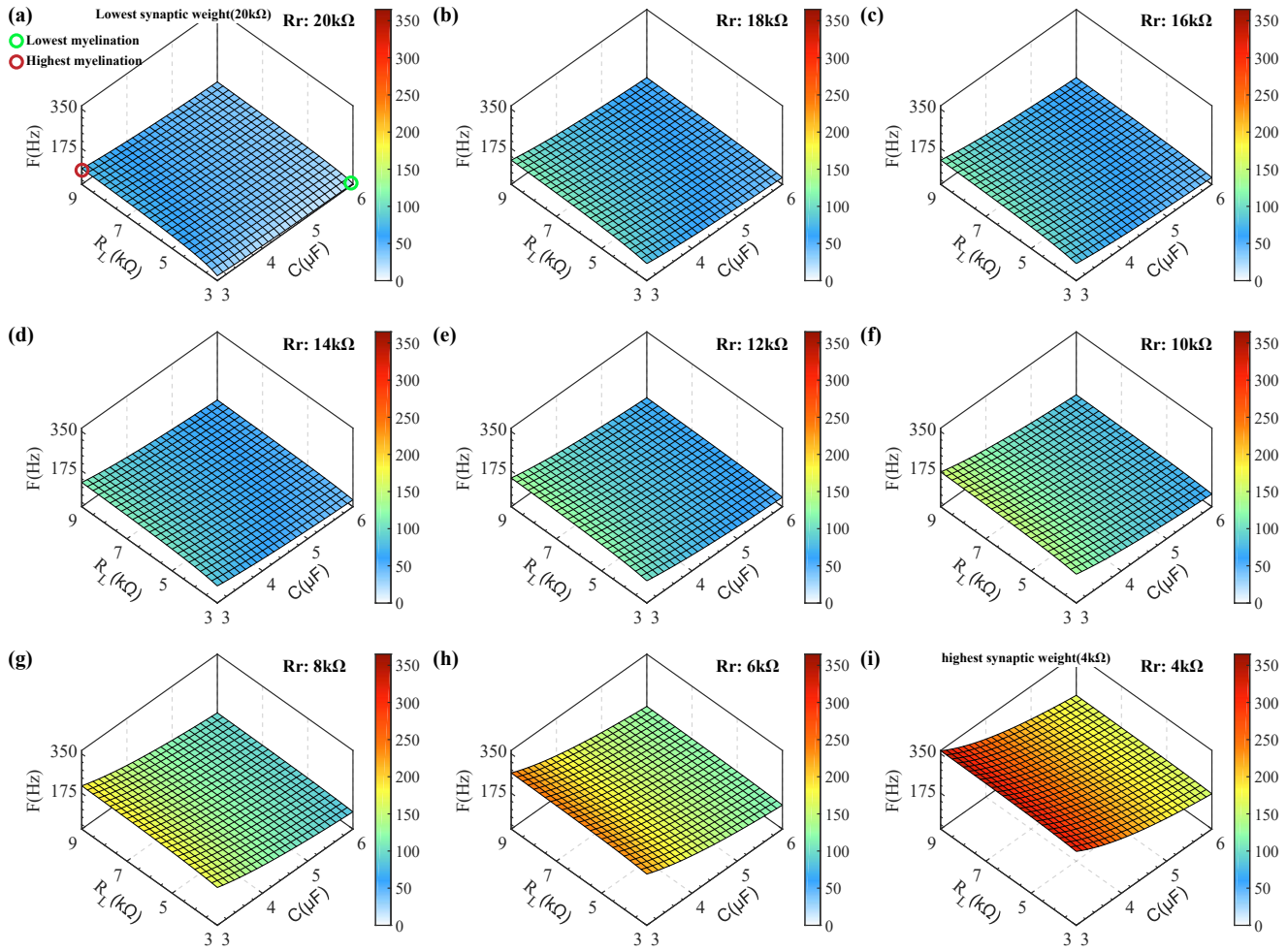


Fig. 10. The synergistic effect of synaptic plasticity and myelin plasticity on the spike firing frequency of neuronal circuits.

only requires adjustments to membrane capacitance and membrane permeability, reducing the number of parameters to be regulated and allowing for more precise tuning of the spike firing frequency at specific nodes in the neuromorphic network. Additionally, myelination in neuronal circuits can enhance the response of existing synaptic connections to input stimuli. The synergistic effect of synaptic and myelin plasticity can further expand the range of spike firing frequency adjustments in the neuronal circuit, as shown in Fig. 10(a) and Fig. 10(i).

In summary, firstly, synaptic and myelin plasticity can regulate the spike firing frequency of neural circuits. Secondly, regulating through synaptic plasticity involves more parameters and is more difficult, while regulating through myelin plasticity involves fewer parameters and results in more precise adjustments. Finally, the synergistic effect of synaptic and myelin plasticity can further expand the regulation range for the spike firing frequency in neural circuits.

#### E. Potential challenges of circuit integration into neuromorphic networks

The existing analysis has sufficiently demonstrated that synaptic and myelin plasticity can independently modulate the

firing behavior of neuronal circuits through distinct mechanisms, while also preliminarily revealing the potential for their interactive effects. In the following sections, we will further investigate their synergistic regulatory mechanisms, focusing on their influence on neuronal response speed, energy efficiency, and spike frequency modulation, as well as evaluating their potential significance in neuromorphic networks. By comparing Fig. 8, Fig. 9 and Fig. 10 with Fig. 11, it is evident that the synergistic interaction between synapses and myelin significantly expands the regulatory capacity of neuronal circuits in terms of response time, energy consumption, and spike firing frequency. Based on the current parameter settings for synaptic weight and degree of myelination, their combined modulation enables the neuronal response time to be reduced to 2.9% of its initial value, the energy consumption per spike to decrease to 38.4% of the original level, and the spike firing frequency to increase to 1982.6% of the initial state.

Shortening the response time of neuron nodes can enhance the neural network's sensitivity to transient disturbances or low-intensity signals, thereby broadening its effective sensing range to some extent and improving perception accuracy. Neuromorphic networks can adaptively regulate the energy

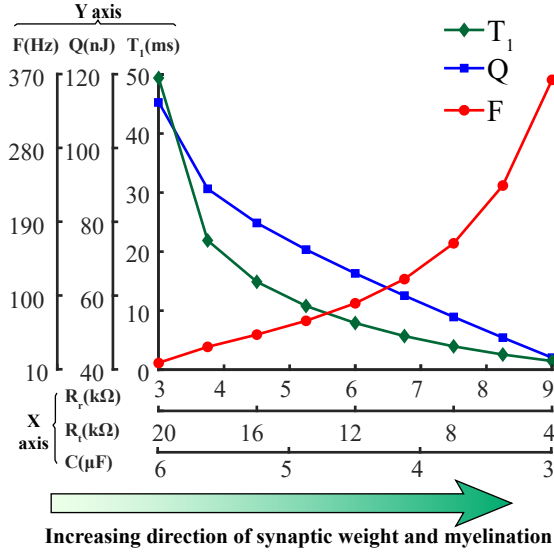


Fig. 11. Schematic diagram illustrating the effects of synaptic and myelin plasticity, and their interaction, on the firing characteristics of neuronal circuits.

consumption of individual spikes at high-frequency firing neuron nodes based on the plasticity of synapses and myelin sheaths, as well as the neurons' discharge history (including count and frequency), thereby reducing the overall energy consumption of the network. An increase in the baseline firing rate of neurons implies that the network as a whole can transmit and process information at a higher speed. Based on the existing synaptic connectivity, modulating the baseline firing rate of neuron nodes can lead to the formation of new network functions or accelerate the processing speed of existing functions.

Subthreshold oscillations (Fig. 12(b)) refer to small-amplitude, aperiodic fluctuations of the membrane potential below the firing threshold, driven by intermittent synaptic inputs and dynamic ionic gradients across the neuronal membrane. Neuron nodes in neuromorphic network exhibit persistent threshold oscillations, posing challenges to the setting of fundamental neuronal parameters. As shown in Fig. 12(a), when a single isolated neuron is stimulated independently by persistently opening AMPA receptor ion channels (shaded region), the intervals between spikes in its continuous spike train are relatively uniform, appearing as a single point in Inter-Spike Interval (ISI) plot (Fig. 13). Introducing white noise can induce sustained subthreshold oscillations in neuron nodes, simulating their state within large-scale neuromorphic networks. As shown in Fig. 12(b), the intervals between spikes in the neuron's spike train become irregular, and the single concentrated point in the ISI plot disperses into a uniformly distributed cloud of points. Neither myelination nor adjustments to synaptic weights can eliminate this phenomenon; they can only reduce the variability of spike intervals, thereby narrowing the distribution range of points in the ISI plot. Furthermore, under constant synaptic connectivity and weights, the sensitivity of neurons to minor perturbations significantly increases with the degree of myelination. Intermittent synaptic

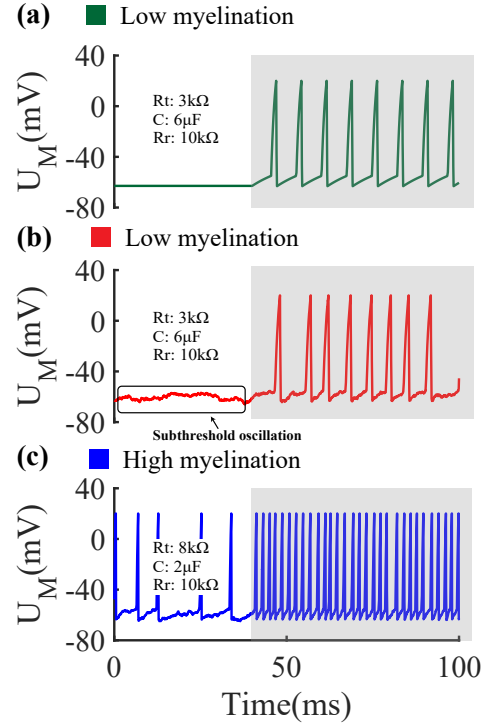


Fig. 12. The impact of noise signals on neuron circuits.

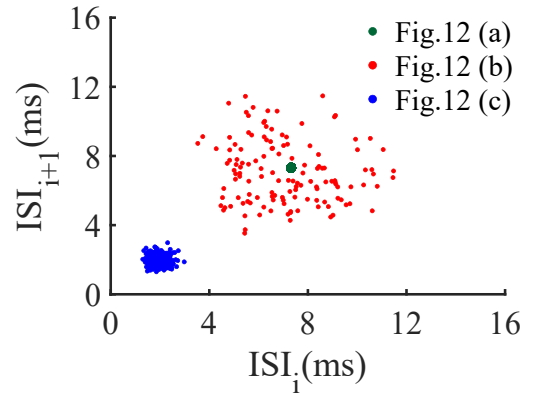


Fig. 13. ISI profiles of neurons with different degrees of myelination under noisy environments.

inputs, which are initially insufficient to trigger firing, can be amplified—when combined with dynamic fluctuations in ion concentration gradients—to elicit spike generation, as shown in Fig. 12(c).

Excessive myelination may lead to frequent firing of neuron nodes, which not only disrupts information transmission and processing within the network but also significantly increases the system's energy consumption. Therefore, when constructing a neuromorphic network based on neuron circuit nodes, the synaptic weights and myelination parameters should be carefully designed according to the network scale, the intensity of threshold oscillations at the nodes, and the intended network function, in order to avoid the adverse effects of over-modulation.

## VI. CONCLUSION

This paper proposes a neuron model that incorporates both synapses and myelin, designs the corresponding neuronal circuit, and introduces a method for quantifying its discharge characteristics. Through theoretical analysis, simulation, and physical experiments, we have validated the effectiveness of this firing characteristic quantization method. We focused on analyzing the impact of synaptic plasticity, myelin plasticity, and their synergistic effects on the response speed, power consumption, and spike firing frequency of neuronal circuits. In the future, we will further investigate the role of myelin plasticity in modulating spike signal transmission speed and improve the analysis of the synergistic effects of synaptic and myelin plasticity in neuromorphic networks.

## REFERENCES

- [1] D. Chen, P. Peng, T. Huang and Y. Tian, "Fully Spiking Actor Network With Intralayer Connections for Reinforcement Learning," *IEEE Transactions on Neural Networks and Learning Systems.*, vol. 36, no. 2, pp. 2881-2893, 2025.
- [2] C. D. Schuman, S. R. Kulkarni, M. Parsa, J. P. Mitchell, P. Date, B. Kay, "Opportunities for neuromorphic computing algorithms and applications," *Nature Computational Science.*, vol. 2, no. 1, pp. 10-19, 2022.
- [3] D. Ham, H. Park, S. Hwang, K. Kim, "Neuromorphic electronics based on copying and pasting the brain," *Nature Electronics.*, vol. 4, no. 9, pp. 635-644, 2021.
- [4] S. Yang, J. Wang, X. Hao, H. Li, X. Wei, B. Deng and K. A. Loparo, "BiCoSS: Toward Large-Scale Cognition Brain With Multigranular Neuromorphic Architecture," *IEEE Transactions on Neural Networks and Learning Systems*, vol. 33, no. 7, pp. 2801-2815, 2022.
- [5] S. Yang, B. Deng, J. Wang, H. Li, M. Lu, Y. Che, X. Wei and K. A. Loparo, "Scalable Digital Neuromorphic Architecture for Large-Scale Biophysically Meaningful Neural Network With Multi-Compartment Neurons," *IEEE Transactions on Neural Networks and Learning Systems*, vol. 31, no. 1, pp. 148-162, 2020.
- [6] M. Yao, O. Richter, G. Zhao, N. Qiao, Y. Xing, D. Wang, T. Hu, W. Fang, T. Demirci, M. De Marchi, L. Deng, T. Yan, C. Nielsen, S. Sheik, C. Wu, Y. Tian, B. Xu and G. Li, "Spike-based dynamic computing with asynchronous sensing-computing neuromorphic chip," *Nature Communications*, vol. 15, no. 1, pp. 4464, 2024.
- [7] N. Rath, I. Chakraborty, A. Kosta, A. Sengupta, A. Ankit, P. Panda, and K. Roy, "Exploring neuromorphic computing based on spiking neural networks: Algorithms to hardware," *ACM Computing Surveys*, vol. 55, no. 12, pp. 243:1-243:49, 2023.
- [8] M. Davies, A. Wild, G. Orchard, Y. Sandamirskaya, G. A. Fonseca Guerra, P. Joshi, P. Plank, and S. R. Risbud, "Advancing neuromorphic computing with Loihi: A survey of results and outlook," *Proceedings of the IEEE*, vol. 109, no. 5, pp. 911-934, 2021.
- [9] Q. Deng, C. Wang, and G. Yang, "Chaotic dynamics of memristor-coupled Tabu learning neuronal network," *International Journal of Bifurcation and Chaos*, vol. 35, no. 05, pp. 2550053, 2025.
- [10] S. Schmidgall, R. Ziaei, J. Achterberg, L. Kirsch, S. P. Hajiseyedrazi, J. Eshraghian, "Brain-inspired learning in artificial neural networks: A review," *APL Machine Learning*, vol. 2, no. 2, pp. 021501, June 2024.
- [11] Q. Deng, C. Wang, and G. Yang, "Generalization and differentiation of affective associative memory circuit based on memristive neural network with emotion transfer," *Neural Networks*, vol. 188, pp. 107502, 2025.
- [12] S. Zhu, T. Yu, T. Xu, H. Chen, S. Dustdar, S. Gigan, D. Gunduz, E. Hossain, Y. Jin, F. Lin, B. Liu, Z. Wan, J. Zhang, Z. Zhao, W. Zhu, Z. Chen, T. S. Durrani, H. Wang, J. Wu, T. Zhang, and Y. Pan, "Intelligent computing: The latest advances, challenges, and future," *Intelligent Computing*, vol. 2, pp. 0006, 2023.
- [13] M. Saponati, M. Vinck, "Sequence anticipation and spike-timing-dependent plasticity emerge from a predictive learning rule," *Nat Commun.*, vol. 14, no. 1, pp. 4985, 2023.
- [14] Y. Andrade-Talavera, A. Fisahn, A. Rodríguez-Moreno, "Timing to be precise? An overview of spike timing-dependent plasticity, brain rhythmicity, and glial cells interplay within neuronal circuits," *Mol Psychiatry.*, vol. 28, no. 6, pp. 2177-2188, 2023.
- [15] X. Duan, Z. Cao, K. Gao, W. Yan, S. Sun, G. Zhou, Z. Wu, F. Ren, B. Sun, "Memristor-Based Neuromorphic Chips," *Adv. Mater.*, vol. 36, pp. 2310704, 2024.
- [16] S. Kumar, X. Wang, J. P. Strachan, Y. Yang, W. D. Lu, "Dynamical memristors for higher-complexity neuromorphic computing," *Nat Rev Mater.*, vol. 7, pp. 575-591, 2022.
- [17] H. Ling, D. A. Koutsouras, S. Kazemzadeh, Y. van de Burgt, F. Yan, p. Gkoupidenis, "Electrolyte-gated transistors for synaptic electronics, neuromorphic computing, and adaptable biointerfacing," *Appl. Phys. Rev.*, vol. 7, pp. 011307, 2020.
- [18] W. Yao, C.H. Wang, Y.C. Sun, S.Q. Gong, and H.R. Lin. "Event-triggered control for robust exponential synchronization of inertial memristive neural networks under parameter disturbance," *Neural Networks.*, vol. 164, pp. 67-80, 2023.
- [19] Z. Deng, C. Wang, H. Lin and Y. Sun, "A Memristive Spiking Neural Network Circuit With Selective Supervised Attention Algorithm," *IEEE Transactions on Computer-Aided Design of Integrated Circuits and Systems.*, vol. 42, no. 8, pp. 2604-2617, 2023.
- [20] Q. Xia, J.J. Yang, "Memristive crossbar arrays for brain-inspired computing," *Nat. Mater.*, vol. 18, pp. 309-323, 2019.
- [21] Y. Peng, H. Wu, B. Gao, J. Tang, Q. Zhang, W. Zhang, J. J. Yang, H. Qian, "Fully hardware-implemented memristor convolutional neural network," *Nature.*, vol. 577, no. 7792, pp. 641-646, 2020.
- [22] D. R. McNeal, "Analysis of a Model for Excitation of Myelinated Nerve," in *IEEE Transactions on Biomedical Engineering*, vol. BME-23, no. 4, pp. 329-337, 1976.
- [23] A. A. Verveen and H. E. Derksen, "Fluctuation phenomena in nerve membrane," in *Proceedings of the IEEE*, vol. 56, no. 6, pp. 906-916, 1968.
- [24] E. Frede, H. Zadeh-Haghighi and C. Simon, "Optical Polarization Evolution and Transmission in Multi-Ranvier-Node Axonal Myelin-Sheath Waveguides," in *IEEE Transactions on Molecular, Biological, and Multi-Scale Communications*, vol. 10, no. 4, pp. 613-622, 2024.
- [25] X. Li, J. Sun, W. Ma, Y. Sun, C. Wang and J. Zhang, "Adaptive Biomimetic Neuronal Circuit System Based on Myelin Sheath Function," *IEEE Transactions on Consumer Electronics*, vol. 70, no. 1, pp. 3669-3679, 2024.
- [26] A. Chawla, S. Morgera, A. Snider, "On Axon Interaction and Its Role in Neurological Networks," *IEEE/ACM Trans. Comput. Biol. Bioinform.*, vol. 18, no. 2, pp. 790-796, 2021.
- [27] Z. Padamsey, D. Katsanevaki, N. Dupuy, N.L. Rochefort, "Neocortex saves energy by reducing coding precision during food scarcity," *Neuron.*, vol. 110, no. 2, pp. 280-296, 2022.
- [28] K. D. Longden, T. Muzzu, D. J. Cook, S. R. Schultz, and H. G. Krapp, "Nutritional state modulates the neural processing of visual motion," *Curr Biol.*, vol. 24, no. 8, pp. 890-895, 2014.
- [29] H. H. Wong, A. J. Watt, P. J. Sjöström, "Synapse-specific burst coding sustained by local axonal translation," *Nature.*, vol. 112, no. 2, pp. 264-276.e6, 2024.
- [30] G. Q. Bi, M. M. Poo, "Synaptic modifications in cultured hippocampal neurons: dependence on spike timing, synaptic strength, and postsynaptic cell type," *J Neurosci.*, vol. 18, no. 24, pp. 10464-72, 1998.
- [31] M. M. Edward, "Intelligence and brain myelination: A hypothesis," *Personality and Individual Differences.*, vol. 17, no. 6, pp. 803-832, 1994.
- [32] F. Wang, S. Y. Ren, J. F. Chen, K. Liu, R. X. Li, Z. F. Li, B. Hu, J. Q. Niu, L. Xiao, J. R. Chan, and F. Mei, "Myelin degeneration and diminished myelin renewal contribute to age-related deficits in memory," *Nature Neuroscience*, vol. 23, no. 4, pp. 481-486, 2020.
- [33] A. R. Raphael and W. S. Talbot, "New insights into signaling during myelination in zebrafish," *Current Topics in Developmental Biology*, vol. 97, pp. 1-19, 2011.
- [34] S. Pan, S. R. Mayoral, H. S. Choi, J. R. Chan, and M. A. Kheirbek, "Preservation of a remote fear memory requires new myelin formation," *Nature Neuroscience*, vol. 23, no. 4, pp. 487-499, Apr 2020.
- [35] J. Li, T. G. Miramontes, T. Czopka, and K. R. Monk, "Synaptic input and  $Ca^{2+}$  activity in zebrafish oligodendrocyte precursor cells contribute to myelin sheath formation," *Nature Neuroscience*, vol. 27, no. 2, pp. 219-231, 2024.
- [36] I. Hong, J. Kim, T. Hainmueller, D. W. Kim, J. Keijsers, R. C. Johnson, S. H. Park, N. Limjunyawong, Z. Yang, D. Cheon, T. Hwang, A. Agarwal, T. Cholvin, F. M. Krienen, S. A. McCarroll, X. Dong, D. A. Leopold, S. Blackshaw, H. Sprekeler, D. E. Bergles, M. Bartos, S. P. Brown, R. L. Hugarir, "Calcium-permeable AMPA receptors govern PV neuron feature selectivity," *Nature*, vol. 635, no. 8038, pp. 398-405, 2024.
- [37] Y. Andrade-Talavera, A. Fisahn, A. Rodríguez-Moreno, "Timing to be precise? An overview of spike timing-dependent plasticity, brain rhythmicity, and glial cells interplay within neuronal circuits," *Mol Psychiatry.*, vol. 28, no. 6, pp. 2177-2188, 2023.

- micity, and glial cells interplay within neuronal circuits,” *Mol Psychiatry*, vol. 28, no. 6, pp. 2177-2188, 2023.
- [38] K. W. Altman and R. Plonsey, “Point source nerve bundle stimulation: effects of fiber diameter and depth on simulated excitation,” *IEEE Transactions on Biomedical Engineering*, vol. 37, no. 7, pp. 688-698, 1990.
- [39] A. L. Hodgkin, A. F. Huxley, “A quantitative description of membrane current and its application to conduction and excitation in nerve,” *J Physiol.*, vol. 117, pp. 500-544, 1952.
- [40] T. W. Rosahl, M. Geppert, D. Spillane, “Short-term synaptic plasticity is altered in mice lacking synapsin I,” *Cell*, vol. 75, no. 4, pp. 661-670, 1993.
- [41] J. Z. Tsien, P. T. Huerta, S. Tonegawa. Spillane, “The essential role of hippocampal CA1 NMDA receptor-dependent synaptic plasticity in spatial memory,” *Cell*, vol. 87, no. 7, pp. 1327-1338, 1996.
- [42] Y. P. Tang, E. Shimizu, G. R. Dube, C. Rampon, G. A. Kerchner, M. Zhuo, G. Liu, J. Z. Tsien, “Genetic enhancement of learning and memory in mice,” *Nature*, vol. 401, no. 6748, pp. 63-69, 1999.
- [43] D. van Blooijis, M. A. van deen Boom, J. F. van der Aar, G. M. Huiskamp, G. Castegnaro, M. Demuru, W. J. E. M. Zweiphenning, P. van Eijsden, K. J. Miller, F. S. S. Leijten, and D. Hermes, “Developmental trajectory of transmission speed in the human brain,” *Nat Neurosci.*, vol. 26, no. 4, pp. 537-541, 2023.
- [44] C. C. H. Cohen, M. A. Popovic, J. Klooster, M. T. Weil, W. Möbius, K. A. Nave, M. H. P. Kole, “Saltatory Conduction along Myelinated Axons Involves a Periaxonal Nanocircuit,” *Cell.*, vol. 180, no. 2, pp. 311-322.e15, 2020.
- [45] L. A. Osso, K. A. Rankin, J. R. Chan, “Experience-dependent myelination following stress is mediated by the neuropeptide dynorphin,” *Neuron.*, vol. 109, no. 22, pp. 3619-3632.e5, 2021.
- [46] W. Yi, K. K. Tsang, S. K. Lam, X. Bai, J. A. Crowell, and E. A. Flores, “Biological plausibility and stochasticity in scalable VO2 active memristor neurons,” *Nature Communications*, vol. 9, no. 1, pp. 4661, 2018.
- [47] X. Li, J. Sun, Y. Sun, C. Wang, Q. Hong, S. Du, J. Zhang, “Design of Artificial Neurons of Memristive Neuromorphic Networks Based on Biological Neural Dynamics and Structures,” *IEEE Transactions on Circuits and Systems I: Regular Papers*, vol. 71, no. 5, pp. 2320-2333, 2024.
- [48] Q. Xu, Y. Wang, H. H.-C. Iu, N. Wang, H. Bao, “Locally active memristor based neuromorphic circuit: Firing pattern and hardware experiment,” *IEEE Transactions on Circuits and Systems I: Regular Papers*, vol. 70, no. 8, pp. 3130-3141, 2023.



**Xiaosong Li** received the B.S. degree from Mechanical Design, Manufacturing, and Automation, Jimei University (JMU), Xiamen, China, in 2017 and the M.S degree from Mechanical Manufacturing, and Automation, Southwest Forestry University, Kunming, China, in 2021. Currently, he is working toward the Eng.D. degree in Energy and Power at College of Computer Science and Electronic Engineering, Hunan University, Changsha 410082, China, and Chongqing Research Institute, Hunan University, Chongqing 401120, China. His research

interests include cognitive neuroscience, memristive logic circuits, and neuromorphic networks.



**Jingru Sun** graduated from Hunan University, China, in 2014 with a Ph.D. degree in computer science and technology. She is an associate professor in College of Computer Science and Electronic Engineering, Hunan University, Changsha, 410082, and Chongqing Research Institute, Hunan University, Chongqing 401120, China. She has published more than 30 papers and her research interests include memristive neural networks, brain-like computing, and intelligent transportation.



**Yichuang Sun** (M'90-SM'99) received the B.Sc. and M.Sc. degrees from Dalian Maritime University, Dalian, China, in 1982 and 1985, respectively, and the Ph.D. degree from the University of York, York, U.K., in 1996, all in communications and electronics engineering. He is currently a Professor of Communications and Electronics, Head of Communications and Intelligent Systems Research Group, and Head of Electronic and Electrical Engineering at the University of Hertfordshire, UK. Professor Sun's expertise and interests are uniquely in the integration

of electronics, communications and computing. He has been conducting active research in wireless and mobile communications, 5G and 6G technologies, RF systems and circuits, analogue and mixed-signal circuits, memristor circuits and systems, neural networks, machine learning, and neuromorphic computing. He has published some 400 papers in peer reviewed journals and conferences and contributed 10 chapters in edited research books. He has also published 4 texts and research books. Professor Sun serves on several Technical Committees of IEEE Circuits & Systems Society and IEEE Communications Society. He has been/is Book Series Editor of an IEE book series, Editor of 8 IEEE and international journals, and sole or lead Guest Editor of over 10 IEEE and IEE/IET journal special issues. He has been on the technical/scientific programme committee of numerous IEEE and international conferences in various roles. Professor Sun has been awarded many national and international awards, prizes, and honours.



**Jiliang Zhang** received the Ph.D. degree in Computer Science and Technology from Hunan University, Changsha, China in 2015. From 2013 to 2014, he worked as a Research Scholar at the Maryland Embedded Systems and Hardware Security Lab, University of Maryland, College Park. From 2015 to 2017, he was an Associate Professor with Northeastern University, China. In April 2017, he joined the Hunan University. He is currently a Full Professor at the College of Integrated Circuits, Hunan University. He is Vice Dean of the College of Integrated Circuits

at Hunan University, the Director of Chip Security Institute of Hunan University, and the Secretary-General of CCF Fault Tolerant Computing Professional Committee. His current research interests include Hardware Security, Integrated Circuit Design and Intelligent System. He has authored more than 60 technical papers in leading journals and conferences. He was the recipient of CCF Integrated Circuit Early Career Award and the winner of Excellent Youth Fund of the National Natural Science Foundation of China. He is serving as a steering member for Hardware Security Forum of China. He is a senior member of IEEE/CCF.